Assessment of Continuous Flow Analysis (CFA) for High-Precision Profiles of Water Isotopes in Snow Cores

Remi Dallmayr[1], Hannah Meyer[2], Vasileios Gkinis[3], Thomas Laepple[5,6], Melanie Behrens[1], Frank Wilhelms[1,4] and Maria Hörhold[1]

[1]Alfred-Wegener-Institut Helmholtz-Zentrum für Polar-und Meeresforschung, Bremerhaven, Am Handelshafen 12, 27570 Bremerhaven, Germany
[2]Institute of Meteorology and Climate Research (IMK-TRO), Department Troposphere Research, Karlsruhe Institute of Technology (KIT), PO 3640, 76021 Karlsruhe, Germany
[3]Niels Bohr Institute Physics of Ice, Climate and Earth, Tagensvej 16, 2200 Copenhagen, Denmark
[4]GZG Abt. Kristallographie, University of Göttingen, Göttingen, Germany
[5]Alfred-Wegener-Institut Helmholtz-Zentrum für Polar-und Meeresforschung, Potsdam, Telegrafenberg A45, 14473 Potsdam, Germany
[6]University of Bremen, MARUM – Center for Marine Environmental Sciences and Faculty of Geosciences, 28334 Bremen, Germany

Correspondence to: Remi Dallmayr (remi.dallmayr@awi.de)

Abstract. In order to derive climatic information from stable water isotopes of the very recent past, the signal-to-noise ratio in climate reconstructions from ice cores has to be improved. To this end, the understanding on the formation and preservation of the climate signal in stable water isotopes at the surface is required, which in turn depends on a substantial amount of snow surface profiles. However, due to its high porosity and poor stability surface snow has been rarely measured, i.e. climate records from firn and ice cores often start at several meter depths and the few discrete samplings of surface snow took large efforts.

We here present a new set-up to efficiently measure stable water isotopes in snow profiles utilizing a Continuous Flow Analysis system enabling measuring multiple snow-cores in a reasonable time and with high-quality. The CFA-setup is described and a systematic assessment of the mixing of the isotope signal due to the set-up is conducted. We systematically determine the mixing length at different parts of the system. We measure and analyse six snow cores from Kohnen station, Antarctica, and find the largest contribution to mixing to originate in the percolation of meltwater on top of the melt head. In comparison to discrete measurements, we show, that our CFA system is able to reasonably analyse highly porous snow cores for stable water isotopes. Still we recommend for future developments to improve the melt head with respect to the strong percolation.

~~An efficient measurement of stable water isotopes in snow profiles is required to improve our understanding of the climate signal preserved in polar firn and ice and to improve the signal to noise ratio in climate reconstructions from ice cores. To allow the analysis of snow cores, we modified a Continuous Flow Analysis system at AWI to analyze multiple snow cores in a reasonable time and with high-quality. We here describe the CFA-setup and isotope measurements, including the methodology to quantify the mixing of the isotope signal induced by the system along its different steps, leading to smoothing of the final isotopic signal. With our obtained mixing lengths for the instrumental setup and the continuous analyze of snow-~~

1 Introduction

Stable water stable isotopes (δ^{18}O and δD) in polar ice cores are commonly used to derive paleo-temperatures (Jouzel et al., 1997). In low accumulation areas of the East Antarctic ice Ice sheetSheet, the reconstruction of past climates over large time scales, i.e. several interglacial periods are possible (e.g., Petit et al., 1999; Kawamura et al., 2017), while at the same time the reconstructions of shorter time scales, i.e. interannual-to decadal climate variabilityies, is highly problematic (Ekaykin et al., 2002; Hoshina et al., 2014; Münch and Laepple, 2018). The reason lies in the large stratigraphic noise (Fisher et al., 1985) imposed by (post-) depositional processes such as wind-redistribution, adding non-climatic variability to the local climate record. In fact, ice core records from most areas on the East Antarctic Plateau are dominated by noise (Laepple et al., 2018, Casado et al.,2020). However, recent studies (Münch et al. 2016, 2017) showed that averaging over a large number of independent vertical profiles allows for inferring a common local climate signal from the stacked stable water isotope record. These findings imply, that it needs a high number of high-resolution snow profiles at an ice core drill site in order to quantify the noise. Commonly, snow profiles were sampled manually at a snow pit trench wall or recently by a snow liner technique (Schaller et al., 2016), where snow cores are extracted from the snow pack and are cut manually into discrete samples. However, by increasing the number of necessary snow cores for each site, the work load for the analysis of discrete samples for their isotopic composition is increasing beyond a feasible manner.

To this end the previously applied Continuous Flow Analysis (hereafter CFA) for ice cores can serve as a solution, as ice cores do not have to be cut prior to analysis, but can be melted and analyzed in oneas a single piece. By continuously melting a longitudinal section of a core sample on a chemically inert melt head, the CFA provides high-resolution measurements of stable water isotopes at high-pace (Gkinis et al., 2011; Dallmayr et al., 2016; Jones et al., 2017) in parallel with other proxies such as concentrations of chemical impurities (Osterberg et al., 2006; Bigler et al., 2011). However, in the past, firn and ice cores were analyzed only starting in several meter depth. Due to the very high porosity and poor stability of surface snow, the upper meter of the polar snow pack has not been analyzed by CFA, but was occasionally sampled discreetly. One obstacle for measurements with CFA is the strong percolation taking place in the highly porous snow. We here refer to "percolation" as the upward movement of meltwater into the snow due to capillary effects. The percolation in the snow above the melt head leads to mixing of melt water of adjacent snow layers. This physical mixing inevitably leads to a smoothing of the derived snow record including the isotope signal (Gkinis et al., 2011). such system is commonly not used with shallow firn and snow cores due to the percolation occurring during the melting within the highly porous samples. A first successful approach to

apply CFA to snow-cores is the LISA Box (Kjaer et al., 2021) for measurements in the field, where a snow core of 10 cm-diameter and 1 m-length is melted on a specifically developed ~~MH~~melt head. Here the meltwater is analyzed for conductivity and peroxide, allowing a quick estimation of age and accumulation rate with high quality. But due to its application in the field, measurements of other parameters such as stable water isotopes are not possible with this set-up.

In order to ~~be able to measure~~enable stable water isotopes measurements in snow cores by CFA, we modified the melting unit of our CFA-system developed at the Alfred-Wegener-Institut, Helmholtz-Zentrum für Polar- und Meeresforschung (hereafter AWI) ~~using~~ to use the ~~MH~~ melt head proposed by Kjaer et al. (2021). We ~~developed~~ systematically assess ~~a method to characterize on a routine base~~ the performance and the mixing of the CFA system with respect to the isotope signal by (1) means of isotopic standards, and (2) comparison to discrete measurements. We here refer to mixing as the alteration of the isotope record (~~as~~originally preserved in the snow) due to the CFA system. ~~Doing so, we~~We were able to separate and quantify the contribution of different components of the CFA to the overall mixing of the isotope signal, and show that the percolation above the melt head is the major contributor.

2. Material and method

2.1. Experimental set-up

The system to analyze 1-meter snow-cores consists of a melting unit adapted to the snow cores geometry, a degassing unit, an electrical conductivity unit, a water isotope measurement unit, a micro-particles detection unit, a fraction collector module, and a data~~sets~~ synchronization system (Fig. 1). The ~~MH~~ melt head is constructed such, that it separates the potentially contaminated outer part of the snow core from the clean inner part. The melt water of the outer part of the snow core is drained to an extra collection unit for non-sensitive measurement, while the melt water of the inner part is driven to the degassing unit (hereafter Debubbler, Fig. 1) by a peristaltic pump (PP in Fig. 1, Ismatec IPC) through a perfluoroalkoxy ~~(PFA)~~ tubing with 1/16" outer diameter ~~(OD)~~ and 0.76 mm inner diameter ~~(ID)~~. Downstream of the ~~DB~~dDebubbler, a second peristaltic pump (Ismatec IPC) drives the now bubble-free water stream to a polyether ketone ~~(PEEK)~~ ~~manifold~~ Manifold (P-150, Idex), from where sub-streams are distributed to the different analytical units through ~~PFA~~ the perfluoroalkox tubing ~~of various inner diameters~~(0.51 mm ~~ID~~inner diameter). Via using the Injection Valve (Fig. 1), ~~During periods where no sample is melted,~~ the analytical units are fed with ultrapure water (Millipore Advantage, Milli-Q ≥ 18.2 MΩ.cm-1, hereafter MQ)~~-~~ during periods where no sample is melted.
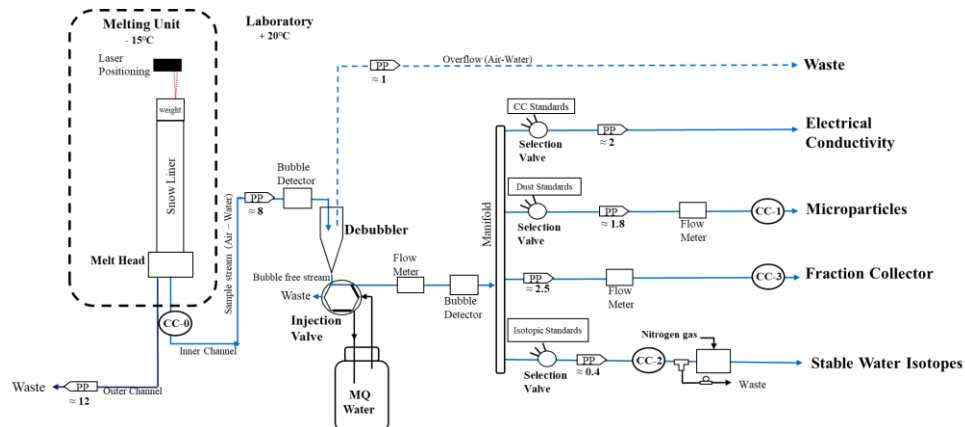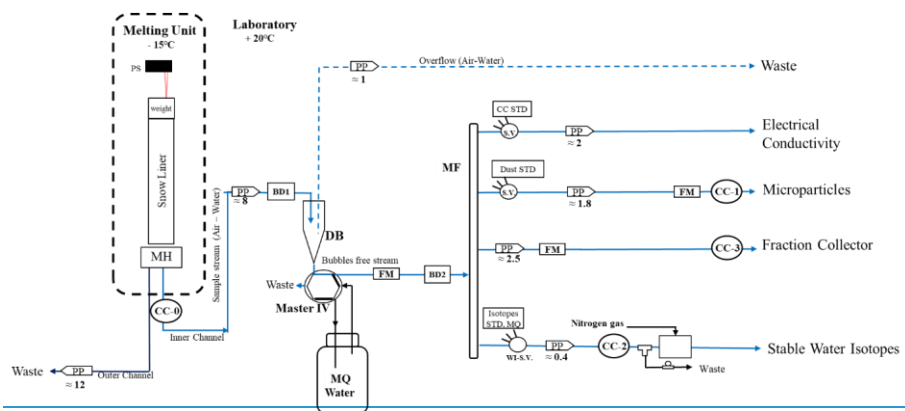
Figure 1: Setup of the AWI-CFA system to measure snow cores. ~~Acronyms refer to the designation in the figure.~~ The snow-core is held in a snow sample holder ~~(SSH)~~ and melted on a Melt-Head ~~(MH)~~ in a -15°C environment (left hand side). The laser positioning sensor ~~(PS)~~ determines the distance to the weight ~~(W)~~ placed on the top of the core. In the laboratory, the conductivity detectors for synchronization (CC-i); an ~~injection~~ Injection V~~v~~alve ~~(Master IV)~~ switching between MQ water and ~~ice~~ snow sample; a degassing unit (~~DB~~Debubbler); a ~~m~~Manifold ~~(MF)~~; ~~selection~~ Selection ~~valves~~ Valves (SV) for analytical units switching between ~~MQ,~~ sample, and standards. The detection of air bubbles takes place upstream and downstream of the Debubbler via using Bubble Detectors. ~~All analytical measurements are indicated.~~ Liquid flow sensors ~~(FM)~~ monitor the flow behaviour of the system. ~~Finally, detection of air bubbles takes place upstream (BD1) and downstream (BD2) of the DB.~~ Finally, Peristaltic Pumps (PP) carry the streams from the melt head to all analytical units. All indicated flow values are expressed in ml min-1. A detailed scheme of the water isotopes line is given in Fig. A1.

~~Snow core~~ **Melting unit** adapted for snow cores

4

The melting unit for snow cores features a 10 cm inner diameter and 120 cm long tube made of acrylic and positioned centrally above the ~~MH~~ melt head (Fig. 2a), guiding the sample during the experiment. A light weight (~150 g) is placed atop of the snow core to stabilize the melt-flow, and is covered on both sides with a 1 mm thickness layer of ~~PTFE~~ ~~t~~Teflon to prevent contamination. Following the work of Dallmayr et al. (2016), a high-accuracy laser positioning senor (Way-con, LLD-150-RS232-50-H) determines the distance from the sensor and the top of the weight with a precision of 0.1 mm in order to derive accurate melt-speeds and to assign precise depths to the datasets generated.
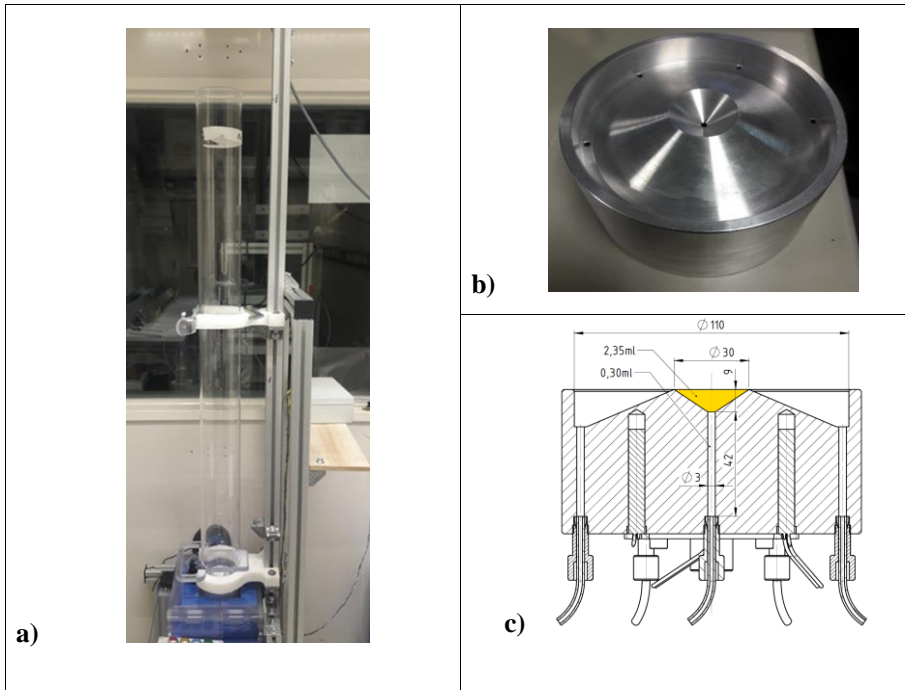
Figure 2: Melting Unit. a) Setup of the snow core melting unit. b) picture of the PICE design ~~MH~~ of the melt head (Kjaer et al., 2021) c) Schematic view of the ~~MH~~melt head, showing the dimension of the inner-channel concave volume (orange).

The ~~MH~~ melt head for snow-cores (Fig. 2b) is based on the Physics of Ice, Climate and Earth, (Copenhagen, Denmark, hereafter PICE) design used by Kjaer et al. (2021), made of aluminum, and manufactured at the AWI in Bremerhaven, Germany. Through a concave volume at the inner-channel (highlighted in Fig. 2c), the shape of the ~~MH~~ melt head prevents

5

120 mixing of clean meltwater from the inner-part with the potentially contaminated outer-part of the core sample. The temperature of the ~~MH~~ melt head is regulated by a Proportional-Integrated-Derivative (PID) temperature controller (JUMO corporate, Germany) attached to eight 125 W heating cartridges and a conventional thermocouple type J.

~~Debubbling~~ Degassing Unit

125 As air in the sample stream leads to significant effects and interferences in the liquid detectors, a separation of air and liquid via a ~~debubbling unit (hereafter d~~Debubbler~~,~~ (Fig. 1) ~~DB in Fig. 1)~~ is required. The incoming flow drips into a micropipette opened to the air, releasing the air bubbles to the atmosphere by buoyancy and leading to a bubble-free flow downstream. Furthermore, regarding the inhomogeneous distribution of air bubbles in the incoming flow, and unpredictable stops of the core melt, maintaining an amount of water in the ~~debubbler~~ Debubbler (safety volume) is essential. To that aim, an overflow-

130 tube (Fig. 1) connected to a peristaltic pump is continuously sucking air, or an overflow if the water-level within the pipette gets in contact. We set the height of this overflow-tube to a minimal safety volume of ~1 ml. A bubble detector located upstream of the unit (Fig. 1) monitors the variability of air in the incoming stream. A second bubble detector is located downstream of the unit (Fig. 1), monitoring, warning and recording the detection of air.

135 **Analytical measurements**

The CFA-system performs the online measurement of electrical conductivity (conductivity-cell model 3082, Amber Sciences Inc., USA, Breton et al., 2012) and micro-particles counting and sizing (Abakus, Klotz GmbH, Germany, Ruth et al., 2002). Stable water isotopes (δ^{18}O and δD) mixing ratios are continuously measured by a Cavity Ring Down Spectrometer (CRDS, Picarro Inc, USA, Maselli et al., 2013). To obtain the continuity and stability of a micro-flow rate of vapor, as required by the

140 instrument, a stream vaporization module was made based on the original method of Gkinis et al. (2010). A micro-volume tee is used to split a micro-flow into a 50 μm ~~ID~~ inner diameter fused-silica capillary from the incoming stream. The waste line featuring a smaller ~~ID~~inner diameter, a back-pressure is enabled and pushes the micro-flow through the capillary towards the oven where mixing with dry air occurs before injection to the instrument. To control the back-pressure precisely and efficiently, we divided the waste line using a second tee and added to one sub-waste line a 10-turn micro-metering needle valve (Dallmayr

145 et al., 2016). Schematic and technical details of the water isotope line are provided in Appendix A.

In addition to the online measurements, fractions of the melted sample water are carefully collected under a laminar flow bench for further offline measurements of chemical impurities by Ion Chromatography (normative precision of <10 %, Göktas et al., 2002).

Additional electrical conductivity measurements are performed at the melting unit outlet (CC-0 in Figure 1, Amber Sciences

150 model 1056, USA) as well as near the inlet of each detection unit (CC-1 to -3 in Fig. 1, contactless conductivity measurement, Edaq, Australia). Such duplicated measurements allow for a straightforward and efficient synchronization of the different data sets during data processing (Dallmayr et al., 2016).

6

Control, ~~and~~ data acquisition and processing~~, processing system, analysis of diffusion~~

All devices are connected to the controlling computer, using a software developed with LabVIEW 2012. Drivers are either provided by manufacturers (pumps, flowmeters) or developed to suit the purpose (Laser positioning, actuated valves, bubble~~s~~ detectors, all analytical units). Analytical data are recorded every second, and are processed after the experiment by using a ~~second piece of software also~~self-made code developed with LabVIEW 2012.

2.2 Assessment of mixing

~~-~~The determination and calculation of the mixing of the stable water isotope signal ~~analyzes of isotopic diffusion are~~was realized using algorithms developed with the software R (R Core Team, 2018).

~~2.2.~~ Characterization of mixing using step functions

CFA-systems are known to diffuse, mix and attenuate the original isotope signal (Gkinis et al., 2011; Jones et al., 2017). The resulting smoothing of the original signal can be described as a mathematical convolution:

$$\delta_m(t) = [\delta_0 \circledast G](t) = \int \delta_0(\tau)G(t-\tau)d\tau \tag{1}$$

~~With~~ with δ_m the measured value and δ_0 the original (isotopic) value of the sample at time t. G is a smoothing filter denoting the impulse response of the system and $\circledast$ refers to the convolution operation.

We here address the characterization of this mixing by analyzing the impulse response of the system (Fig. 4), i.e. we analyze the derivative of the response of the system to an instantaneous (step) isotopic change. Previously two approaches have been proposed to treat the step response:

First, Gkinis et al. (2011) fit this so-called step response of the system to a scaled cumulative distribution function (hereafter CDF) of a normal distribution, as:

$$\delta_{normal}(t) = \frac{A}{2}\left[1 + erf\left(\frac{t-t_0}{\sigma\sqrt{2}}\right)\right] + B \tag{2}$$

with A and B the isotopic values of the step scaled, t_0 the initial time, and σ the standard deviation. All parameters are determined by means of least square optimization. In the case of a normal distribution, the impulse response of the CFA-system is described by a Gaussian impulse probability density function (hereafter PDF):

$$G_{normal}(t) = \frac{1}{\sigma_{normal}\sqrt{2\pi}}e^{-\frac{(t-t_0)^2}{2\sigma_{normal}^2}} \tag{3}$$

Here, the standard deviation of the Gaussian PDF (σ_{normal}) characterizes the mixing length of the system, expressed in seconds. Later, these values can be converted into a mixing length expressed in mm by applying the measured melt-speed.

Second, because of the skewed shape of the impulse response, Jones at al. (2017) proposed an implementation from normal CDF to two multiplied lognormal CDFs ($\delta_{log-log}(t) = \frac{C}{2}\left[1 + erf\left(\frac{t-t_1}{\sigma_1*\sqrt{2}}\right)\right]\left[1 + erf\left(\frac{t-t_2}{\sigma_2\sqrt{2}}\right)\right] + D$). This approach provides a

185　slightly better fit to the signal, but the diffusion length is then retrieved using an additional function, fitting the two lognormal CDFs. The derived mixing length requires thus a careful interpretation due to these additional uncertainties.

Our results show very small differences in the resulting mixing lengths obtained by the different approaches (Table 2). We therefore focus this work on the straight forward Gaussian approach to determine the diffusion lengths and assessment of contribution to the overall mixing. s computed with the straightforward Gaussian approach. We apply both approaches,
190　compare the results and assess the contribution of the different CFA units to the overall mixing length using the Gaussian distribution.

2.3 Characterization of mixing by comparison to discrete Snow-core samplessamples

To evaluate the mixing and the overall performances of the CFA-system, we compare the results obtained from CFA
195　continuous analysis with discretely measured samples from the same snow cores. via six 1-meter long snow cores (KF13 to KF18). We use six 1-meter long snow cores (with the names KF13 – to KF 18), The snow cores originatinge from Kohnen station (0°04E 75°00 S, 2892 m.a.s.l.), Dronning Maud Land (Oerter et al., 2009). This area is characterized by an accumulation rate of 75 mm w.e. yr^{-1} over the last 50 years (Moser et al., 2020). The snow cores were taken following the procedure by Schaller et al, (2016) from a trench wall excavated during the 2014/2015 (Münch et al., 2017) with a horizontal
200　distance of 5m. The snow cores were stored in carbon fibre tubes, sealed with plastic bags (WhirlPaek) on each end, inside a Styrofoam box at -25°C. The 1 -meter average density of these snow cores ranges between season (Münch et al., 2017), where the cores used in this study correspond to an absolute snow depth of 240-340 cm (i.e. a density of 340 – 345 kg.m-3 (Münch et al., 2017).), with a horizontal distance of 5 m. High-resolution density measurements display the layered character of the snow, which induces mm-to-cm variations in density and microstructure. However, stable water isotopes do not capture these
205　variations, as the diffusion on site smoothes the signal rather quickly (Moser et al. 2020).

From all snow cores a calotte of 25 mm thickness lengthwise was cut into discrete samples at 22 mm resolution. From all snow cores a longitudinal section (slice) of 25mm thickness was cut. This slice was further cut into discrete subsamples of 22 mm size in vertical resolution. The discrete samples were analyzed at AWI Potsdam in 2015 (hereafter dataset discrete-15). In 2019, a second discrete dataset was obtained with a similar 22 mm depth-resolution, just prior to the measurement by CFA
210　continuous analysis of the remaining core (55 mm wide). For this second discrete dataset (hereafter discrete-19), four cores (KF13-16) were analyzed for isotopic composition whereas the remaining two cores (KF17 and 18) were analyzed for ion chromatography at AWI Bremerhaven. For the discrete datasets 2015 and 2019, single isotopic measurements are provided with an accuracy of 0.1 ‰ for δ^{18}O, and 1.5 ‰ for δD. For the measurement of the isotopic composition of the disrectediscrete 2019 data set the instruments Picarro L2120-i and Picarro L2130-i were used. The measurement set-up followed the Van-
215　Geldern protocol (Van Geldern and Barth, 2012). Each sample was injected 4 times. As a measure of accuracy, we calculated the combined standard uncertainty (Magnusson et al., 2017) including the long-term reproducibility and bias of our laboratory by measuring a quality check standard in each measurement run and including the uncertainty of the certified standards. The combined uncertainty for δ18O is 0.14 ‰ and for δD is 0.8 ‰.

## 3. Results ~~– Stable Water Isotopes~~

3.1 ~~Instrumental behavior~~Assessing the instrumental performance of the analyzer for stable water isotope measurements

In order to describe the stability and performance of the ~~spectrometer, the~~CRDS instrument for continuous analysis of~~to for~~ stable water isotopes ~~(CRDS, Picarro)~~, a so-called Allan variance test is applied ~~The behavior of the CRDS is determined by Allan variance test~~ (Allan, 1966) where over a period of more ~~longer~~ than 12 hours ~~rs by continuous injection of~~ MQ water~~.~~ ~~is continuously injected at the selection valve for water isotopes~~ (~~figure~~Fig. 1). Such a test allows the investigation of the noise and drift of ~~our s~~the spectrometer with respect to the integration time.

The Allan variance is defined as:

$$A_{var} = \frac{1}{2(n-1)} \sum_{i=1}^{n-1} (y(\tau)_{i+1} - y(\tau)_i)^2 \tag{4}$$

with $y(\tau)$ the average value of the measurements during an integration interval of length τ, and n being the total number of intervals. The results show the linear decrease of the Allan deviation (square root of Allan variance) up to an ~~optimal deviation~~minimal deviation for an integration time of ~6000 s (Fig.3). Instrumental drift starts slightly earlier than ~~104~~10^4 s (Fig.3) with low deviation (0.01 ‰ for δ^{18}O and 0.1 ‰ for δD) up to 4*10^4 s. As one run (melting 1-meter liner with CFA) takes less than 2000 seconds, our measurement- time window of this one meter is well within the non-affected time window for drift. Therefore ~~we run~~ one single calibration for ~~one meter is sufficient~~ each single meter is necessary. ~~, as one calibration seems sufficient~~Therefore, for our snow cores study and the longest single analysis segment of <3000 s, a single calibration per core is necessary.

9
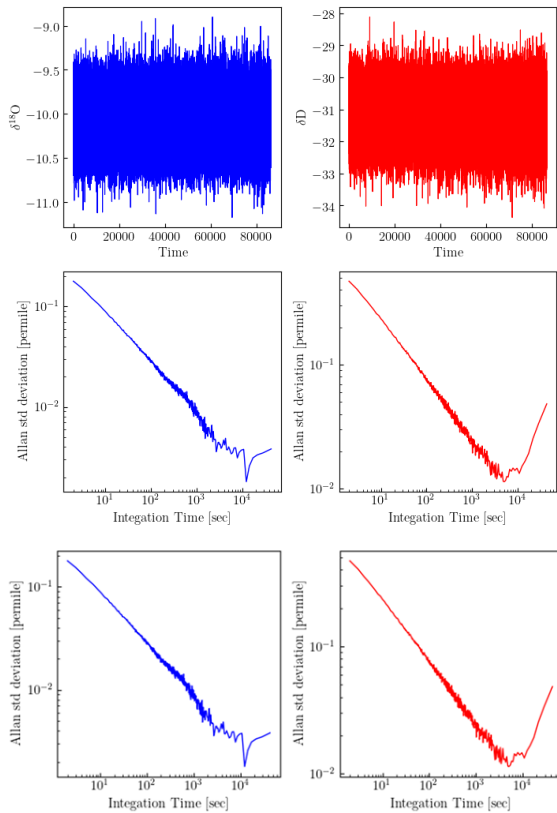
Figure 3: >12 h of Allan deviation analysis for δ^{18}O (left panel, in blue), and δD (right panel, in red).

3.2 Calibration to the VSMOW-~~VSLAP/SLAP~~ scale <u>and deriving the</u> ~~,~~ precision of <u>the</u> continuous dataset

Calibrations of the raw data are performed using 3 <u>in-house</u> laboratory ~~-~~standards (Table 1) which are annually calibrated to the international VSMOW-~~V~~SLAP scale. <u>Each standard is measured for more than 15 minutes by feeding the</u> ~~CFA~~CRDS <u>with the standard water</u> via the ~~master~~isotopic selection valve. The <u>values of the</u> last 2 minutes of each ~~>15 min laboratory standard~~ run ~~is~~ <u>are</u> averaged. <u>The obtained values are plotted against the defined values, the resulting</u> ~~Based on the measured and real~~

10

~~values of the standards, a~~ linear regression fitting the 3 ~~-~~points~~s~~ is applied and defines the calibration coefficients (Fig. B1, Appendix B).

	NZE	TD1	JASE
$\delta^{18}O$	-19.85 (0.02)	-33.85 (0.02)	-50.22 (0.05)
δD	-152.7 (0.3)	-266.2 (0.3)	-392.5 (0.4)

250 **Table 1:** Defined Isotopic composition of the in-house laboratory standards used for VSMOW-SLAP calibrations, in ‰. ~~In brackets t~~ For each standard, the combined uncertainty is given in parenthesis.
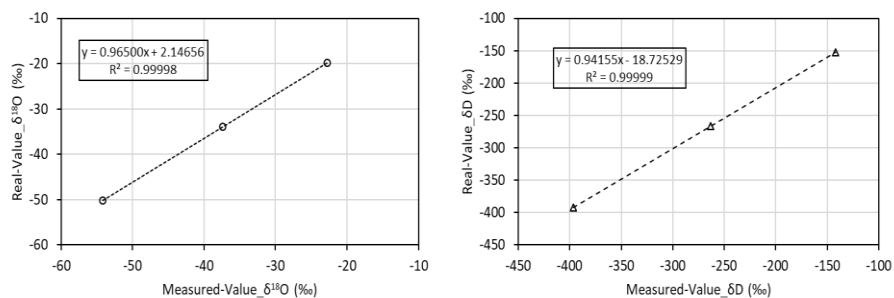

~~Figure 4: VSMOW three-points calibration with laboratory standards NZE, TD1, JASE (left: $\delta^{18}O$, right: δD).~~

255

The precision of the CFA measurements for stable water isotopes is determined from the standard deviation (1 SD) of the last 2 minutes of each injected standard run. ~~In addition to the calibration, the laboratory standards are used to infer the precision of our measurements, defined as the level of internal agreement among independent measures.~~ The derived ~~standard-deviation (1SD)~~ precision from 18 calibration runs ~~of the last 2 minutes of each injected standard~~ (N=18) is ~~of~~ 0.24 ± 0.02 ‰ and 0.47

260 ± 0.04‰ for $\delta^{18}O$ and δD, respectively.

3.3. Mixing ~~induced by the instrumental CFA-system~~length derived from step function tests

We estimate the mixing length by means of isotopic liquid standards through different experiments~~details given in C1, Appendix C~~. First, during each calibration procedure, abrupt isotopic changes are applied at the water isotopes selection valve

265 (dataset CRDS-line, Fig.4). The steps applied here range between ~100 ‰ and ~140 ‰ in Deuterium and did not show any

11

dependency between isotopic step size and resulting diffusion length. In a ~~first~~ second experiment, we applied an isotopic step at the ~~MH~~ melt head (~230 ‰) with its concave volume filled (~~Fig.5,~~ dataset MH-filled, Fig.4)~~N=4experiments MH-filled 1 4~~). The same step ~~is~~ was then applied with the concave volume empty (~~Fig.5,~~ dataset MH-empty, Fig.4). All details of the experiment are given in ~~,~~Appendix C ~~N=4~~), ~~t~~Table C1~~.~~. ~~In addition to these two experiments, during each calibration procedure, abrupt isotopic changes are applied at the water isotopes selection valve (dataset CRDS-line, Fig.5,N=15experiments CRDS-line 9 24).~~
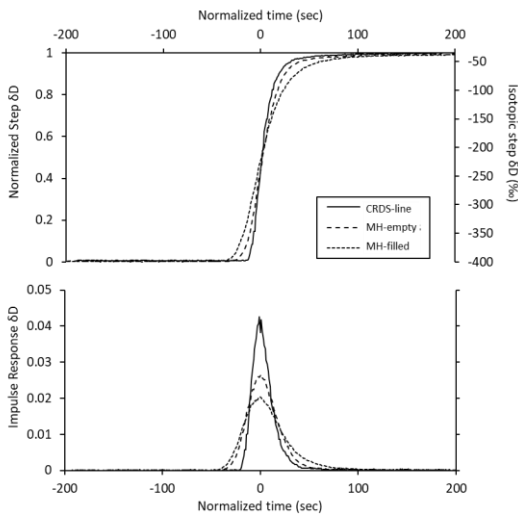

Figure ~~5~~4: Isotopic step and impulse responses obtained for the three experiments realized. ~~Isotopic switch at the isotope selection valve (WI-SV in Fig. 1) or at the Melt-Head (MH, Fig. 1), concave volume filled or empty.~~ Upper panel: The different step function experiments. Lower panel: the corresponding impulse responses.

Using equations (1) to (3), we compute the mixing lengths *(σ)* of our set of experiments (*σMH-filled*, *σMH-empty*, *σCRDS-line*). All results for both isotopologues δD and $\delta^{18}O$ are presented in Table C2, Appendix C. Because the results are ~~Being~~ very similar, we focus our study on the results for δD (Table 2)~~The results for both isotopologues δD and $\delta^{18}O$ are very similar ppendix , and we focus our study on the results for δD (Table 2)~~. Furthermore, in addition to evaluating the mixing length induced by the whole CFA system, the combination of the three datasets allows us to distinguish between the contributions of the different parts of the system. Assuming independent mixings from each other from the ~~Melt~~melt ~~Head~~ head (MH) to the water isotopes

selection valve (WI-SV), and later to the CRDS instrument, the total mixing filter is the sum of the variances of each mixing filter along the CFA-system.

$$\sigma^2_{CFA-system} = \sigma^2_{MH-filled} = \sigma^2_{MH} + \sigma^2_{MH\,to\,WI-SV} + \sigma^2_{CRDS-line} \tag{6}$$

We can evaluate by quadrature difference (1) the mixing length induced by the concave volume of the ~~MH~~ melt head ($\sigma_{MH} = \sqrt{\sigma^2_{MH-filled} - \sigma^2_{MH-empty}}$), as well as (2) the mixing length induced downstream of the ~~MH~~ melt head to the isotopic selection valve ($\sigma_{MH\,to\,WI-SV} = \sqrt{\sigma^2_{MH-empty} - \sigma^2_{CRDS-line}}$).

~~$\sigma_{MH-filled}$~~	~~$\sigma_{MH-empty}$~~	~~$\sigma_{CRDS-line}$~~	~~σ_{MH}~~	~~$\sigma_{MH\,to\,WI-SV}$~~
~~21.6 (2.4)~~	~~14.5 (1.2)~~	~~12.6 (1.8)~~		
~~13.6 (1.5)~~	~~9.2 (0.7)~~	~~8.0 (1.1)~~	~~10.0~~	~~4.5~~

~~**Table 2:** δD means mixing length derived from the normal PDF, expressed in seconds (italic) and in mm (bold). Values in parenthesis represent 1SD. The conversion of seconds to mm is based on a melt-speed of 38 mm.min-1. σ_{MH} and $\sigma_{MH\,to\,WI\,SV}$ correspond to differences in quadrature between $\sigma_{MH\,filled}$ and $\sigma_{MH\,empty}$, and between $\sigma_{MH\,empty}$ and $\sigma_{CRDS\,line}$, respectively.~~

	$\sigma_{MH-filled}$	$\sigma_{MH-empty}$	$\sigma_{CRDS-line}$	σ_{MH}	$\sigma_{MH\,to\,WI-SV}$
Skew	20.0 (1.9)	13.7 (1.1)	11.5 (2.2)		
	12,7 (1.2)	**8.7 (0.7)**	**7.3 (1.4)**	**9.2**	**4.7**
Normal	21.6 (2.4)	14.5 (1.2)	12.6 (1.8)		
	13.6 (1.5)	**9.2 (0.7)**	**8.0 (1.1)**	**10.0**	**4.5**

Table 2: δD mean~~s~~ mixing length~~s~~ derived from the skew and normal PDFs, expressed in seconds (italic) and in mm (bold). Values in parenthesis represent 1SD. The conversion of seconds to mm is based on a melt-speed of 38 mm.min-1. σ_{MH} and $\sigma_{MH\,to\,WI-SV}$ correspond to differences in quadrature between $\sigma_{MH-filled}$ and $\sigma_{MH-empty}$, and between $\sigma_{MH-empty}$ and $\sigma_{CRDS-line}$, respectively.

We find a total mixing length of the AWI CFA system of ~14 mm (Table 2), indicating that the majority of the instrumental mixing is induced by the concave volume of the PICE design ~~MH~~ melt head (10 mm mixing length), closely followed by the CRDS-line (8 mm). The tubular section in between, composed of tubes and the ~1ml safety volume of the debubbler, shows a significantly smaller contribution (4.5 mm).

13

3.4. Snow-core continuous records versus discrete records
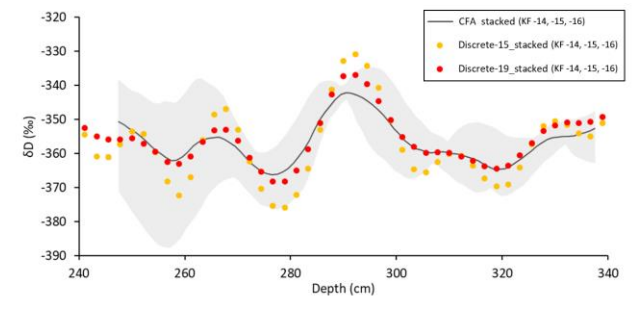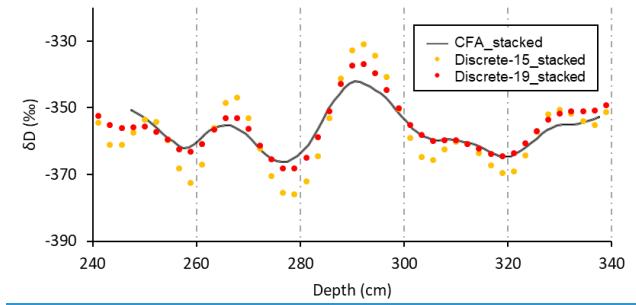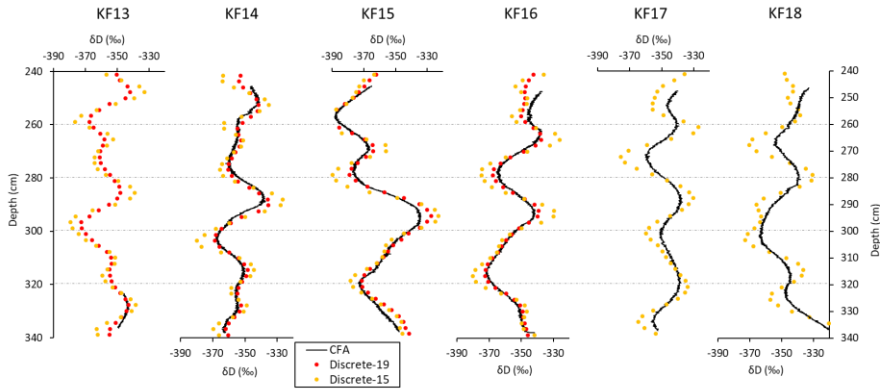
Figure 65: Isotopes profiles of the 6 snow cores. ~~Top~~Upper panel: 240-340 cm depth δD profiles of the six cores, 5 meters spaced. Datasets of continuous measurement (black lines), discrete-15 (orange markers) and discrete-19 (red markers) are shown. Because of the transition from MQ to sample and vice-versa, we removed the top-70 mm and bottom-20 mm of the continuous dataset. Note the small 150 mm portion of reliable continuous analysis for the core KF13, due to issues during the run. The averaged melt-speed of the 6 runs is 38 mm.min-1 (1SD = 9 mm.min-1).
~~Bottom~~Lower panel: Mean datasets of the stacked CFA (black) and discrete (dotted) profiles of the snow cores KF-14, -15, -16. The gray shaded area displays the ~~spatial variability~~spread of the three CFA profiles. ~~(shade area) is indicated by the spread of the three continuous profiles.~~

3.4 Mixing length derived from comparison to discrete measurements

We compare the discrete values from 2015 and 2019 as well as the values obtained from CFA at the single profiles (Fig. 65, upper panel) as well as at the mean profile, averaged over all profiles (Fig. 6 5 bottom) and quantify the differences. We first observe a mismatch in the depth assignment between discrete and CFA values – i.e., the phase of the records has an off-set of 12.3± 6.4 mm. One reason for the mismatch could be the short-term fluctuation in the melt speed induced by density variations. However, the melt speed is measured with high resolution and variations are included in the depth assignment. We therefore assume that the major source of uncertainty is the general linkage between discretely cut samples and continuous measurements. ~~The reason can be small-scale variations in density, leading to short-term changes in the melt-speed and thus affecting the depth-assignment of the CFA values.~~ Secondly, comparing the amplitude between isotopic minima and maxima show that the continuous record attenuates on average ~17% of the discrete-19 record, and ~48% of the discrete-15 record. The strong difference between the two discrete datasets reveal a further and significant diffusional process occurring likely during the storage of the snow cores (Van der Wel et al., 2011). Therefore, we use the discrete-19 dataset to assess the ~~mixing of the CFA~~ effect of percolation. ~~(section 3.4.1 / hereafter?), and the~~, while ~~t~~The off-set between the two discrete data-sets ~~2015 and 2019~~ is discussed later as an indicator of diffusion during storage (discussion, supplement). ~~discrete -15 dataset to investigate / discuss? the effect of long-term storage on snow cores (section 3.4.2 4.3).~~

~~3.4.1 Mixing induced by continuous analysis of snow-core samples~~Separating the effect of percolation from the overall mixing

When continuously analyzing a snow-core, due to the high-porosity of the upper-meters samples, capillary action (Colbeck, 1974) forces the melted water at the MH to lift upwards, enabling percolation (Fig. 76). Thus, by comparing the continuous dataset with a percolation-free discrete dataset, we aim to assess the mixing induced by the percolation.
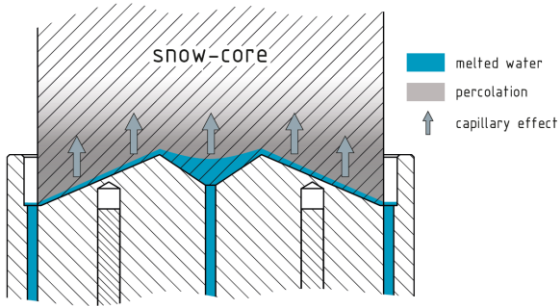
Figure ~~7~~6: Illustration of the melting experiment showing the percolation induced by the low density of the sample combined to the melt-water reservoir within the inner concave volume of the ~~MH~~melt head.

In order to retrieve the mixing length induced by the continuous analysis of snow-cores with respect to the discrete dataset, we convolved the discrete signal with a family of impulse responses of different mixing lengths. A set of discrete-convolved signals of flattened extrema are obtained, and each signal is compared to the CFA signal (previously smoothed on 22 mm to ensure the same averaging than the discrete samples). Then, the minimum of root-mean-square (RMS = $\sqrt{mean\left(\left(x_i - x_j\right)^2\right)}$) between convolved signals and the continuous record allows for the identification of the adequate mixing length $\sigma_{CFA\text{-}discrete}$.

	KF13	KF14	KF15	KF16	KF17	KF18
$\sigma_{CFA-discrete19}$ Normal-CDF	x	29	32	31	x	x
$\sigma_{CFA-discrete15}$ Normal-CDF	x	49	52	57	56	57

Table 3: Mixing lengths (in mm) of the continuous profiles of δD, as related to the discrete-19 dataset and to the discrete-15 dataset. No results are available for the core KF13 due to the too short continuous dataset.

We find ~~an~~ average mixing length~~s~~ of approximately 30 mm ~~using with~~for the discrete 2019 dataset, and 54 mm ~~with~~for the discrete 2015 dataset (Table 3). Following equation (6), we separate the mixing from the percolation at the ~~MH~~melt head from the remaining CFA system by:

$$\sigma^2_{CFA-discrete(19)} = \sigma^2_{CFA-system} + \sigma^2_{percolation} \tag{7}$$

16

$\sigma_{CFA\text{-}discrete19(t)}$ refers to the overall mixing retrieved from the convolution of the discrete 2019 signal. $\sigma_{CFA\text{-}system}$ is the observed mixing of 14mm of the CFA system derived from experiments with the step function (section 3.3).

By retrieving the quadratic difference of CFA-discrete19 – CFA system, we can compute the mixing length induced by the percolation at the ~~MH~~ melt head with ~27 mm. This length is twice the length induced by the experimental system. Thus,
360 percolation is the limiting factor on retrieved signal resolution when applying CFA on snow cores.

3.4.2. Smoothing of the isotope signal due to storage

We find a difference between the two discrete datasets 2015 and 2019 at the same snow cores, alongside with a mean $\sigma_{CFA\text{-}discrete15}$ value of ~54 mm (Table 3).

This difference is not related to instrumental induced mixing, but indicates the effect of long-term storage of snow samples.
365 We assume, that the diffusion, taking place in snow and firn (Gkinis et al., 2014) is active in the cold store as well. Using our results, we can now quantity this storage-induced diffusion. Assuming that the mixing of the discrete-15 dataset corresponds to the mixing of the discrete-19 dataset convolved with an independent smoothing filter induced by the storage, comes:

$$\sigma^2_{CFA-discrete15} = \sigma^2_{CFA-discrete19} + \sigma^2_{storage\ 15-19} \tag{8}$$

Using the retrieved mixing lengths $\sigma_{CFA\text{-}discrete19}$ = 30 mm and $\sigma_{CFA\text{-}discrete15}$ = 54 mm, we derive a diffusion length of
370 approximately 45 mm. These findings indicate, that during the 4 years of storage (first analysis in 2015 – versus second analysis in 2019) the isotope signal in the snow cores is smoothed by this diffusion length.

We further computed for each 1-meter long snow core the mean and variability (standard deviation) of the both discrete datasets (Table 4). The decrease in variability indicates an averaged attenuation of 0.54 ‰ and 4.5 ‰ for $\delta^{18}O$ and δD, respectively.
375 The changes in the means show an averaged enrichment of isotopic composition of +0.31 ‰ for $\delta^{18}O$ and +1.6 ‰ for δD, likely due to the repeated contact with laboratory-air when bags are opened, and the loss of sample (frost) in the bag (personal communication, Sepp Kipfstuhl).

> **Commented [MH1]:** Moved to discussion

4. Discussion

The need to address local spatial noise in the stable water isotope ice core records from low-accumulation rate areas such as
380 Kohnen station, Dronning Maud Land, with an accumulation rate of 200-300 mm recent annual gain of snow (Münch et al.,

17

2017) motivates to analyze low-density snow cores with less efforts compared to discrete sampling. In order to assess the ability of a CFA system to analyze these very low density (e.g. (<400 kg.m^{-3}, Laepple et al., 2016) cores we here ~~applied~~used ~~With the~~an adapted melting unit of the ~~newly developed~~ CFA system ~~for snow cores~~ we measured ~~in~~to ~~anaylze~~ in total 6 snow cores from ~~the same location,~~Kohnen station. We find a ~~retrieving a~~ good agreement between the different isotope profiles of the different snow cores. ~~measurements. We find that a large portion of the smoothing of the isotope signal originates from the percolation at the inner concave volume of the PICE design MH. 2.However, despite this limitation,~~ Tthe derived mixing length of the ~~performances of our current CFA~~experimentalCFA system with ~~regards~~ respect to the δD isotopic signal ~~diffusion are~~ is found to be similar to the improved CFA-CRDS system at University of Colorado (mixing length for δD of 21.6 seconds, section 3.3 of this work, versus 19.1 seconds, Jones et al., 2017). These agreements in derived mixing lengths indicate, together with our quantitative estimates (tTable 2), that a major contribution to the mixing is inherent in the usage of the Picarro instrument (CRSD line) ~~and its cavity.~~

~~ityT4As the obtained mixing lengths do not show any similar trend (see Table 3), we can state that the mixing length is not sensitive to melt speed variations. We however observed a significant variability of melt speed within each core (between 10 and 20 % of the mean speed, Table 5), likely related to the variations of density along each snow core.~~

	KF13	KF14	KF15	KF16	KF17	KF18
~~Average speed~~	~~x~~	~~28.7~~	~~31~~	~~33~~	~~46~~	~~49.5~~
~~Standard deviation~~	~~x~~	~~3.8 (13%)~~	~~4.4 (14%)~~	~~5.6 (17%)~~	~~9 (19%)~~	~~5.3 (11%)~~

~~**Table 4:** Melt speed statistics for the different snow cores, expressed in mm.min^{-1}. The upper row shows the averaged melt speed of each run, while the lower row indicates the corresponding variability (standard deviation observed in mm.min-1), and in parenthesis as a percentage of the mean value.~~

4.1 Suggestion to ~~Aa~~dressing the ~~p~~Percolation at the melt head

The ~~other (quantitative~~largest) contribution originates from the percolation at and above the melt head. We assign the percolation to the design of the melt head with and its large inner concave volume (Fig. 2). ~~Its application to low density cores (<400 kg.m^{-3}, Laepple et al., 2016) from low accumulation rate areas (Kohnen station, 200-300 mm recent annual gain of snow, Münch et al., 2017) gives relevant insights to the isotopic variations in spite of limitations in the measurements of their amplitudes.~~

To overcome the high-level of mixing induced by the percolation, it is crucial to prevent the formation of a reservoir of melt-water in contact with the snow-core, specifically in the inner volume at the ~~MH~~melt head. Thus, a new design of inner channel offers a possibility towards this aim. A flat surface covered with boreholes will allow for an efficient and uniform evacuation of the melt-water, limiting the suction upward. In addition to addressing the percolation, such design will significantly increase

410 the experimental performances (section 3.3) in order to ultimately offer the necessary quality to resolve reliably the full isotopic cyclicity in the snowpack in low accumulation rate areas. ~~Concerning very low accumulation rate sites, e.g. Vostock: ~60 mm annual snow layer thickness (Ekaykin et al., 2002); Dome F: ~74 mm (Kameda et al., 2008); Dome C: ~77 mm (Touzeau et al., 2016), additional improvements are necessary.~~ The significant contribution of the Picarro analyzer (CRDS-line~~, ~~(section 3.3) ~~must here~~could be addressed as well, and requires likely a collaboration with the manufacturer to improve the analytical

415 unit itself (e.g. reduction of the large ~~strong increase of~~ volume at its inlet before a pressure-drop to the 40 Torr cavity). ~~We expect the mixing to drop when using a different melt head design, lowering the difference between discrete and continuous CFA data.~~

4.2 The effect of variations of melt speed to the mixing length

420 Further we explored the sensitivity of mixing length to melt speed. We melted the snow cores at different melt speeds, varying from 28.7 mm per minute to 49.5 mm per minute (Table 4). As the obtained mixing lengths do not show any trend~~s~~ (see Table 3), we are confident that the mixing length is not sensitive to melt speed variations. We however observed variability of melt speed within each core between 10 and 20 % of the mean speed (Table 5), which can be related to small-scale variations of snow density or friction within the sample holder.

425

	KF13	KF14	KF15	KF16	KF17	KF18
Average speed	x	28.7	31	33	46	49.5
Standard deviation	x	3.8 (13%)	4.4 (14%)	5.6 (17%)	9 (19%)	5.3 (11%)

Table 4: Melt speed statistics for the different snow cores, expressed in mm.min^{-1}. The upper row shows the averaged melt speed of each run, while the lower row indicates the corresponding variability (standard deviation observed, in mm.min^{-1}), and in parenthesis as a percentage of the mean value.

430

4.3 Spatial variability

The six firn cores were taken in the vicinity of Kohnen station with a distance of 5m. Their different profiles display stratigraphic noise, i.e. spatial variability. The variability in the isotope profiles due to this spatial variability is in the range or larger (Figure 6~~5~~, lower panel) than the error obtained due to the mixing by the CFA, i.e. the reduced amplitudes compared to

435 discrete data or delay in the signal compared to the discrete data. This strengthens the potential in using CFA to analyze many snow cores of one site to generate an average isotope profile (Münch et al, 2017).

4.4 Diffusion of the isotope signal during storage of snow cores

19

As a result of the comparison of the CFA data to discrete measurements (Fig. 5), we observed a significant difference ~~n off-~~ ~~set~~ between the stable water isotopic ~~compositions~~profiles of the same snow cores~~,~~. ~~but~~ sampled at different times. ~~We find a~~ ~~difference between the two discrete datasets 2015 and 2019 at the same snow cores, alongside with a mean~~ $\sigma_{CFA\text{-}discrete15}$ ~~value~~ ~~of ~54 mm (Table 3).~~

This difference is not related to instrumental induced mixing, but indicates the effect of long-term storage of snow samples. We assume, that the diffusion, taking place in snow and firn (Gkinis et al., 2014) is active in the cold store as well. Using our results, we can now quantity this storage-induced diffusion. Assuming that the mixing of the discrete-15 dataset corresponds to the mixing of the discrete-19 dataset convolved with an independent smoothing filter induced by the storage, comes:

$$\sigma^2_{CFA-discrete15} = \sigma^2_{CFA-discrete19} + \sigma^2_{storage\ 15-19} \qquad (8)$$

Using the retrieved mean mixing lengths $\sigma_{CFA\text{-}discrete19}$ = 30 mm and $\sigma_{CFA\text{-}discrete15}$ = 54 mm (Table 3), we derive a diffusion length of approximately 45 mm. These findings indicate, that during the 4 years of storage (first analysis in 2015 – versus second analysis in 2019) the isotope signal in the snow cores is smoothed by this diffusion length.

Additionally, ~~W~~we computed for each 1-meter long snow core the mean and variability (standard deviation) of ~~the~~ both discrete datasets (Table 5). The decrease in amplitude indicates an averaged attenuation of 0.54 ‰ and 4.5 ‰ for $\delta^{18}O$ and δD, respectively. The mean values show on average an enrichment of isotopic composition of +0.31 ‰ for $\delta^{18}O$ and +1.6 ‰ for δD, likely due to the repeated contact with laboratory-air when bags are opened, and the loss of sample (frost) in the bag.

	$\delta^{18}O$	$\delta^{18}O$	δD	δD
	Discrete-15	Discrete-19	Discrete-15	Discrete-19
KF13	-45.29 (1.3)	-45.076 (0.85)	-356.31 (11.93)	-355.77 (8.05)
KF14	-45.14 (1.45)	-44.71 (0.85)	-354.85 (12.24)	-353.12 (7.69)
KF15	-46.38 (2.39)	-45.91 (2.05)	-364.36 (19.53)	-361.51 (16.75)
KF16	-44.95 (1.70)	-44.76 (1.16)	-353.87 (14.72)	-353.30 (10.23)

Table 4~~5~~: $\delta^{18}O$, δD means (standard deviation) for each snow core discrete dataset, expressed in ‰.

~~The observation of the significant smoothing induced by the storage of the core samples is of particular interest.~~ We show ~~in~~ ~~Fig. B1 (Appendix B)~~ the effect of storage on diffusion lengths for both isotopologues (Fig. BD1 Appendix BD) based on firn-

20

diffusion model (Gkinis et al., 2014). Assuming a storage temperature of -20⁰C , ~~aand a low~~ density of 370 kg.m^{-3}, an accumulation rate of 75 mm w.e. yr^{-1}, and a time window of 4 years, a ~~lead to a very similar~~ diffusion length for δD similar to our observations ~~than~~ can be found. As ~~our quantification (section 3.4.3). t~~The diffusivity coefficients are ~~being~~ positively correlated to temperature (Fig. ~~B2~~D2, Appendix ~~B~~D), the diffusion during storage is likely of stronger magnitude than on the East-Antarctic plateau. However, the strength of the observed diffusion during storage is due to the low density of the snow cores and we do not expect such a strong change for firn and ice core samples from greater depth and with higher density.

5. Conclusions

Overcoming the increased stratigraphic noise in low accumulation areas and constraining the isotope signal formation within the upper-firn ~~can be realized, but~~ requires large number of high-quality stacked vertical profiles (Münch et al., 2017). In order to cope with the related challenge of high-pace -quality analysis and paired measurements of various proxies, we present~~ed~~ here a CFA-system, adapted for analysis of snow-cores using ~~the Niels Bohr Institute design of Melt Head~~a previously ~~adapted~~designed melt head for snow cores (Kjaer et al. 2021). Based on standard step functions and mathematical approaches ~~(on standards and the method of~~ Gkinis et al., ~~(~~2011, Jones et al., 2017), we ~~developed algorithms to quantify~~quantify the ~~smoothing~~ mixing of the isotopic signal induced by the CFA system and separate the different ~~inferred its major~~ contributors. As a result, we identify percolation (especially strong due to the low density) at and above the melt head as a major contributor to the overall mixing of the isotope record. Despite these limitations we show that CFA can be used to obtain reasonable isotope profiles of snow cores, keeping information on both, the spatial and temporal variability. However, ~~Using discrete samples, we further investigated and quantified the strong additional smoothing induced by the low density of the snow core samples~~for future applications of CFA to snow cores ~~. In order to offer a reliable high-resolution isotopic record in area of low accumulation rate such as Kohnen station,~~ we recommend a new design of ~~Melt Head~~the melt head, with a focus on the evacuation of the melt-water. ~~For very low accumulation rate sites however, using a CFA technique requires likely additional modification (i.e. mixing induced by the CRDS analytical device itself).~~

Finally, the isotopic diffusion during storage of snow-core samples requires further investigation, but underlines the need of (1) a strategy to preserve the original record (discrete samples cut in the field) or (2) prompt analysis with techniques such as the CFA.

490

21

APPENDIX A: CFA water isotope line
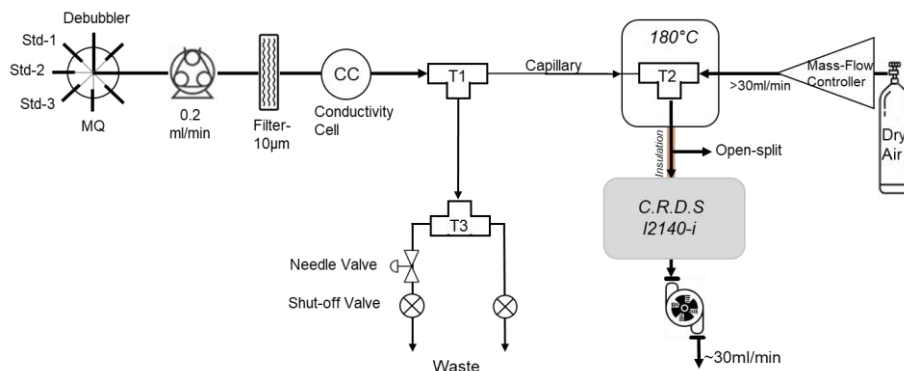
Figure A1: Detailed schematic of water isotopes line of the AWI CFA-system.

The selected sample steam is drained at a flow of ~0.2 ml.min^{-1} through PFA tubes of 0.51 mm ID to a 10 μm frits-filter (A-107, Idex), then a synchronization conductivity cell before entering a stainless-steel micro-volume tee (U-428, Idex; T1 in Fig. S1). Here, a micro-flow is split from the incoming stream into a fused-silica capillary tube (50 μm ID), the rest going into the waste line. Due to the smaller ID of the waste line (0.25 mm ID), a back-pressure pushes the micro-flow through the capillary towards the oven. To control this back-pressure precisely and efficiently, the waste line is divided using a PEEK tee (T3) and added to one of the two sub-waste lines a 10-turn micro-metering needle valve (P-445, Idex).

The sample micro-flow is injected into the stainless-steel tee (T2, Valco ZT1M) mounted in the 180°C oven, where it vaporizes instantly and mixes with a controlled flow of dry air (Mass Flow Controller SEC-E40 N2 100SCCM, Horiba company) to form a gas sample with the desired water vapor concentration.

$y = 0.96500x + 2.14656$
$R^2 = 0.99998$

$y = 0.94155x - 18.72529$
$R^2 = 0.99999$
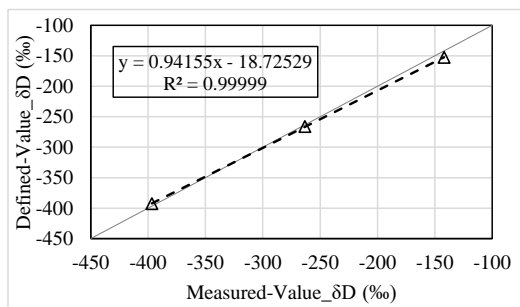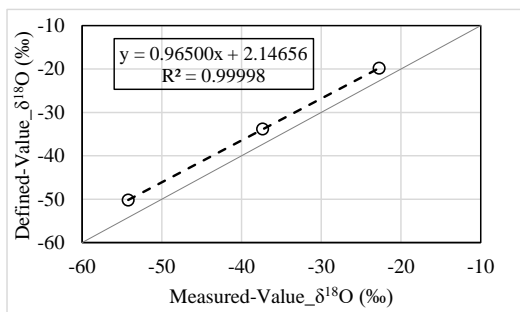
Figure B1: VSMOW three-points calibration with in-house laboratory standards NZE, TD1, JASE. (Upper panel: $\delta^{18}O$, lower panel: δD). ~~I~~Thin black line is the 1:1 line. Datapoints are raw data, i.e. before calibration.

	Value after calibration		Differences with defined value	
	$\delta^{18}O$	δD	$\delta^{18}O$	δD
NZE	-19.804	-152.422	-0.045	-0.278
TD1	-33.935	-266.732	0.084	0.532
JASE	-50.181	-392.247	-0.039	-0.252

Table B1: Deviations between calibrated and defined values ~~after applying the computed regression lines~~. All values are expressed in ‰.

23

Appendix-C: Mixing length derived from step function tests

Experiment	Abbreviation	Number of runs	Standards switch	Isotopic step size
Water Isotopes Calibration (step 1)	CRDS-line	5	MQ to NZE	~100 ‰
Water Isotopes Calibration (step 2)	CRDS-line	5	NZE to TD1	~120 ‰
Water Isotopes Calibration (step 3)	CRDS-line	5	TD1 to JASE	~140 ‰
Melt head filled	MH-filled	4	TD1 to MQ	~ 230 ‰
Melt head empty	MH-empty	4	TD1 to MQ	~ 230 ‰

Table C1: Details of the different experiments conducted to assess the overall instrumental mixing, and separating the different contributions along the setup.

	$\sigma_{MH-filled}$		$\sigma_{MH-empty}$		$\sigma_{CRDS-line}$		σ_{MH}		$\sigma_{MH\ to\ WI-SV}$	
	$\delta^{18}O$	δD	$\delta^{18}O$	δD	$\delta^{18}O$	δD	$\delta^{18}O$	δD	$\delta^{18}O$	δD
Skew	*19.6 (1.8)*	*20.0 (1.9)*	*13.4 (1.2)*	*11.5 (2.2)*	*10.7 (2.2)*	*13.7 (1.1)*				
	12.4 (1.1)	**12,7 (1.2)**	**8.5 (0.8)**	**7.3 (1.4)**	**6.8 (1.4)**	**8.7 (0.7)**	**9.0**	**9.2**	**5.1**	**4.7**
Normal	*20.3 (2.3)*	*21.6 (2.4)*	*13.6 (1.3)*	*14.5 (1.2)*	*11.2 (2.0)*	*12.6 (1.8)*				
	12.9 (1.4)	**13.6 (1.5)**	**8.6 (0.8)**	**9.2 (0.7)**	**7.1 (1.3)**	**8.0 (1.1)**	**9.6**	**10.0**	**4.9**	**4.5**

Table C2: Means mixing length derived from the skew and normal PDFs, expressed in seconds (italic) and in mm (bold) for both $\delta^{18}O$ and δD. Values in parenthesis represent 1SD. The conversion of seconds to mm is based on a melt-speed of 38 mm.min-1. σ_{MH} and $\sigma_{MH\ to\ WI-SV}$ correspond to differences in quadrature between $\sigma_{MH-filled}$ and $\sigma_{MH-empty}$, and between $\sigma_{MH-empty}$ and $\sigma_{CRDS-line}$, respectively.

24

APPENDIX ~~B~~D: Firn diffusion during storage

Density: 370 kgm^{-3}, temperature: 253.15 K
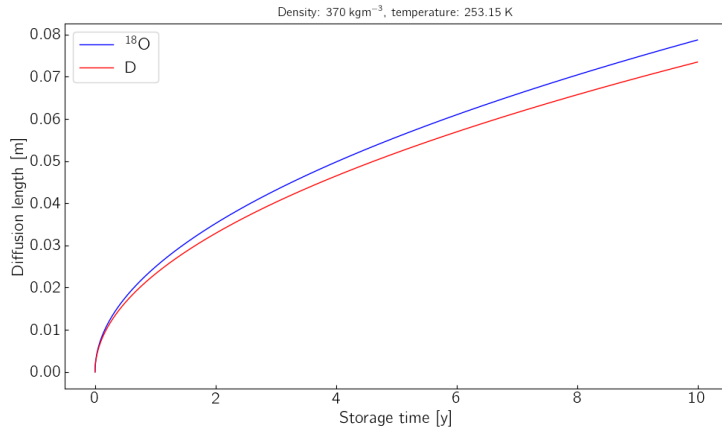
Figure D1: Exemplary f~~F~~irn-diffusion length estiamtes for ~~core samples~~firn samples with a ~~(~~density of 370 kg.m^{-3} ~~)~~ as function of storage time~~the time of storage (-20ºC)~~. The firn diffusion length is computed based on the model by Gkinis et al. (2014), using a temperature of -20ºC and an accumulation rate of 75 mm w.e. yr-1.
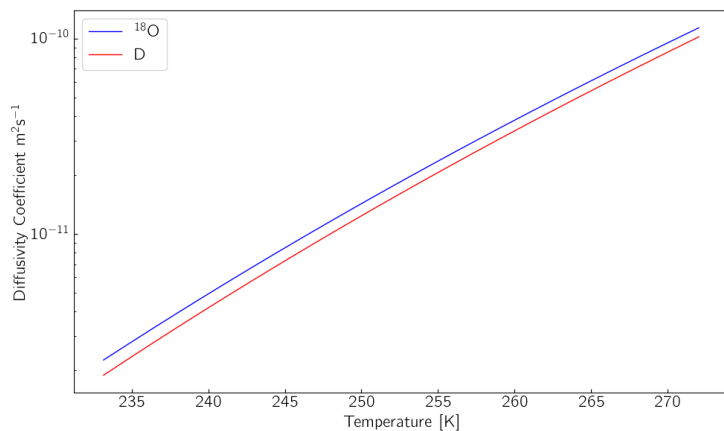
Figure D2: Diffusivity coefficients versus temperature, constraints as ~~above~~above, and displaying the annual mean temperature at Kohnen station (-43⁰C, Weinhart et al., 2020) and the storage temperature (-20⁰C).~~.~~

550

APPENDIX E: Data removed from continuous datasets

	Top	Bottom
KF 13	x	36
KF 14	53	19
KF 15	57	20
KF 16	66	19
KF 17	75	22
KF 18	76	21

Table E1: Data removed from the top (left column), and the bottom (right column) of the continuous datasets due to the transition with MQ water (expressed in mm).

26

555

Authors contribution

RD developed the CFA-system, designed and proceeded to the tests, experiments, analysis, and co-supervised the diffusion characterization tests. HM ~~participated to the~~took part in all experiments and ~~,~~ developed ~~all~~ the algorithms to characterize the isotopic diffusion using the R-software. VG provided the routines to calculate the step functions and the results of the model
560 run to describe diffusion during storage~~provided his expertise on CFA and characterization of isotopic diffusion, and provided insights of the storage effect based on firn diffusion~~. MH developed the research question and supervised the CFA campaigns. Together with TL the scientific background on isotope signal formation in surface snow has been implemented. ~~Through the COMB i project, MH and TL motivated the use of CFA with snow cores.~~ MB conducted all discrete isotopic ~~measurements and~~measurements and the quality check at AWI-Bremerhaven. All authors contributed to the writing of the manuscript.
565 ~~RD developed the CFA-system, designed and proceeded to the tests, experiments, analysis, and co-supervised the diffusion characterization Master thesis. All authors contributed to the writing of the manuscript.~~

Competing interests

The authors declare that they have no conflict of interest.
570

Data availability

The algorithms developed in R to characterize the isotopic diffusion are available at: https://github.com/Ice-core-Paleo-Proxies/AWI_CFA_Isotope. The snow-cores discrete samples isotopic datasets 2015 and 2019 are archived at the PANGAEA database, under https://doi.pangaea.de/10.1594/PANGAEA.939208 and https://doi.pangaea.de/10.1594/PANGAEA.939207,
575 respectively.
The snow-cores continuous high-resolution profiles are archived under https://doi.pangaea.de/10.1594/PANGAEA.969073.
PANGAEA is hosted by the Alfred Wegener Institute Helmholtz Centre for Polar and Marine Research (AWI), Bremerhaven, and the Center for Marine Environmental Sciences (MARUM), Bremen, Germany.

27

References

Allan, D. W.: Statistics of atomic frequency standards, P. IEEE, 54, 221–230, 1966.

Bigler, M.; Svensson, A.; Kettner, E.; Vallelonga, P.; Nielsen, M.E.; Steffensen, J. P.: Optimization of High-Resolution Continuous Flow Analysis for Transient Climate Signals in Ice Cores. Environ. Sci.Technol. 45, 4483−4489, 2011.

Breton, D.J., Koffman, B.G., Kurbatov, A.V., Kreutz, K.J. and Hamilton, G.S.: Quantifying Signal Dispersion in a Hybrid Ice Core Melting System. Environ. Sci. Technol., 46(21), 11922-11928, doi: 10.1021/es302041k, 2012.

Colbeck, S.: The capillary effects on water percolation in homogeneous snow. Journal of Glaciology, 13(67), 85-97. doi:10.3189/S002214300002339X, 1974.

Dallmayr, R., Goto-Azuma, K., Kjær, H. A., Azuma, N., Takata, M., Schüpbach, S. and Hirabayashi, M.: A High-Resolution Continuous Flow Analysis System for Polar Ice Cores, Bull. Glaciol. Res., 34, 11–20, https://doi.org/10.5331/bgr.16R03, 2016.

Drücker, C., Wilhelms, F., Oerter, H., Frenzel, A., Gernandt, H. and Miller, H.: Design, transport, construction, and operation of the summer base Kohnen for ice-core drilling in Dronning Maud Land, Antarctica., Ice drilling technology 2000: Proceedings of the fifth International Workshop on Ice Drilling Technology, 30 October-1 November 2000, Nagaoka University of Technology, Nagaoka, pp. 302-312, 2002.

Ekaykin, A. A., Lipenkov, V. Y., Barkov, N. I., Petit, J. R., and Masson-Delmotte, V.: Spatial and temporal variability in isotope composition of recent snow in the vicinity of Vostok station, Antarctica: implications for ice-core record interpretation, Ann. Glaciol., 35, 181–186, doi:10.3189/172756402781816726, 2002.

Fisher, D. A., Reeh, N., and Clausen, H. B.: Stratigraphic noise in time series derived from ice cores, Ann. Glaciol., 7, 76–83, doi:10.3198/1985AoG7-1-76-83, 1985.

Gkinis, V., Popp, T. J., Johnsen, S. J., and Blunier, T.: A continuous stream flash evaporator for the calibration of an IR cavity ring down spectrometer for isotopic analysis of water, Isot. Environ. Health S., 46, 1–13, 2010.

Gkinis, V., Popp, T. J., Blunier, T., Bigler, M., Schüpbach, S., Kettner, E., and Johnsen, S. J.: Water isotopic ratios from a continuously melted ice core sample, Atmos. Meas. Tech., 4, 2531–2542, doi:10.5194/amt-4-2531-2011, 2011.

Gkinis V., Simonsen S. B., Buchardt S. L., White J. W. C. and Vinther B. M.: Water isotope diffusion rates from the NorthGRIP ice core for the last 16,000 years – glaciological and paleoclimatic implications. Earth Planet. Sci. Lett., 405, 132/141, https://doi.org/10.1016/j.epsl.2014.08.022., 2014.

620 Göktas, F., Fischer, H., Oerter, H., Weller, R., Sommer, S., & Miller, H.: A glacio-chemical characterization of the new EPICA deep-drilling site on Amundsenisen, Dronning Maud Land, Antarctica. Annals of Glaciology, 35, 347-354. doi:10.3189/172756402781816474, 2002.

Hoshina, Y., K. Fujita, F. Nakazawa, Y. Iizuka, T. Miyake, M. Hirabayashi, T. Kuramoto, S. Fujita, and Motoyama, H.: Effect of accumulation rate on water stable isotopes of near-surface snow in inland Antarctica, J. Geophys. Res. Atmos., 119, 274– 283, doi:10.1002/2013JD020771, 2014.

625 Jones, T.R.; White, J.W.C.; Steig, E.J.; Vaughn, B.H.; Morris, V.; Gkinis, V.; Markle, B.R.; Schoenemann, S.W. (2017): Improved methodologies for continuous-flow analysis of stable water isotopes in ice cores, Atmos. Meas. Tech., 10, 617–632, doi.org/10.5194/amt-10-617-2017, 2017.

Jouzel J., Alley, R. B., Cuffey, K. M., Dansgaard, W., Grootes, P., Hoffmann, G., Johnsen, S. J., Koster, R. D., Peel, D., Shuman, C. A., Stievenard, M., Stuiver, M., White, J.: Validity of the temperature reconstruction from water isotopes in ice 630 cores. Journal of Geophysical Research 102(C12), 471–487 doi: 10.1029/97JC01283, 1997.

Kameda, T., Motoyama, H., Fujita, S., and Takahashi, S.: Temporal and spatial variability of surface mass balance at Dome Fuji, East Antarctica, by the stake method from 1995 to 2006, J. Glaciol., 54, 107–116, doi:10.3189/002214308784409062, 2008.

Kawamura, K., Abe-Ouchi A., Motoyama, H., Ageta, Y., Aoki, S., Azuma, N., Fujii, Y., Fujita, K., Fujita, S., and Fukui, K.: 635 State 30 dependence of climatic instability over the past 720,000 years from Antarctic ice cores and climate modeling, Science advances, 3(2), e1600,446, 2017.

Kjaer, H.A., Hauge, L.L., Simonsen, M., Yoldi, Z., Koldoft, I., Hoerhold, M., Freitag, J., Kipstuhl, S., Svensson, A., Vallelonga, P.: A portable Lightweight In Situ Analysis (LISA) box for ice and snow analysis, The Cryosphere, 15, 3719– 3730, 2021 https://doi.org/10.5194/tc-15-3719-2021, 2021.

640 Laepple, T., Hörhold, M., Münch, T., Freitag, J., Wegner, A., and Kipstuhl, S.: Layering of surface snow and firn at Kohnen Station, Antarctica: Noise or seasonal signal? J. Geophys. Res. Earth Surf., 121, 1849–1860, doi:10.1002/2016JF003919, 2016.

Laepple, T., Münch, T., Casado, M., Hoerhold, M., Landais, A., and Kipstuhl, S.: On the similarity and apparent cycles of isotopic variations in East Antarctic snow pits, The Cryosphere, 12, 169–187, https://doi.org/10.5194/tc-12-169-2018, 2018.

Magnusson, B; Näykki, T; Hovind, H; Krysell, M; Sahlin, E: Handbook for calculation of measurement uncertainty in 645 environmental laboratories. *Nordtest Report TR 537 (ed. 4). 2017.*

Maselli, O. J., Fritzsche, D., Layman, L., McConnell, J. R. & Meyer, H.: Comparison of water isotope-ratio determinations using two cavity ring-down instruments and classical mass spectrometry in continuous ice-core analysis. Isotopes Environ. Health Stud. 387–398, https://doi.org/10.1080/10256016.2013.781598, 2013.

Moser, D.E., Hoerhold, M., Kipfstuhl, S., Freitag, J.: Microstructure of Snow and Its Link to Trace Elements and Isotopic
650   Composition at Kohnen Station, Dronning Maud Land, Antarctica. Front. Earth Sci. 8:23. doi: 10.3389/feart.2020.00023,
2020.

Münch, T., Kipfstuhl, S., Freitag, J., Meyer, H., and Laepple, T.: Regional climate signal vs. local noise: a two dimensional
view of water isotopes in Antarctic firn at Kohnen Station, Dronning Maud Land, Clim. Past, 12, 1565–1581,
https://doi.org/10.5194/cp-12-1565-2016, 2016.

655   Münch, T., Kipfstuhl, S., Freitag, J., Meyer, H., and Laepple, T.: Constraints on post-depositional isotope modifications in
East Antarctic firn from analysing temporal changes of isotope profiles, The Cryosphere Discuss., 2017, 1–21, doi:10.5194/tc-
2017-35, 2017.

Münch, T. and Laepple, T.: What climate signal is contained in decadal- to centennial-scale isotope variations from Antarctic
ice cores? Climate of the Past, 14, 2053–2070, doi: 10.5194/cp-14-2053-2018, 2018.

660   Oerter, H., Drücker, C., Kipfstuhl, S., Wilhelms, F.: Kohnen Station - the Drilling Camp for the EPICA Deep Ice Core in
Dronning Maud Land, Polarforschung; 78, 1-2; 1-23, 2009.

Osterberg, E.C., Handley, M.J., Sneed, S.B., Mayewski, P.A. and Kreutz, K.J.: Continuous Ice Core Melter System with
Discrete Sampling for Major Ion, Trace Element, and Stable Isotope Analyses. Environ. Sci. Technol., 40(10), 3355-3361,
doi: 10.1021/es052536w, 2006.

665   Petit, R. J., D. Raynaud, I. Basile, J. Chappellaz, C. Ritz, M. Delmotte, M. Legrand, C. Lorius, L. Pe, J. R. Petit, J. Jouzel, D.
Raynaud, N. I. Barkov, J. M. Barnola, I. Basile, M. Bender, J. Chappellaz, M. Davis, G. Delaygue, M. Delmotte, V. M.
Kotlyakov, M. Legrand, V. Y. Lipenkov, C. Lorius, L. Pepin, C. Ritz, E. Saltzman, and M. Stievenard: Climate and
atmospheric history of the past 420,000 years from the Vostok ice core, Antarctica, Nature, 399(6735), 429–436, 1999.

Ruth, U., D. Wagenbach, M. Bigler, J. P. Steffensen, and R. Röthlisberger, High resolution dust profiles at NGRIP: Case
670   studies of the calcium-dust relationship, Ann. Glaciol., 35, 2002.

Schaller, C. F., Freitag, J., Kipfstuhl, S., Laepple, T., Steen-Larsen, H. C., and Eisen, O.: A representative density profile of
the North Greenland snowpack, The Cryosphere, 10, 1991–2002, https://doi.org/10.5194/tc-10-1991-2016, 2016.

Steinhage, D., Kipfstuhl, S., Nixdorf, U., & Miller, H.: Internal structure of the ice sheet between Kohnen station and Dome
Fuji, Antarctica, revealed by airborne radio-echo sounding. Annals of Glaciology, 54(64), 163-167.
675   doi:10.3189/2013AoG64A113, 2013.

Touzeau, A., Landais, A., Stenni, B., Uemura, R., Fukui, K., Fujita, S., Guilbaud, S., Ekaykin, A., Casado, M., Barkan, E.,
Luz, B., Magand, 20 O., Teste, G., Le Meur, E., Baroni, M., Savarino, J., Bourgeois, I., and Risi, C.: Acquisition of isotopic
composition for surface snow in East Antarctica and the links to climatic parameters, The Cryosphere, 10, 837–852,
doi:10.5194/tc-10-837-2016, 2016.

680   Van der Wel, L., Gkinis, V., Pohjola, V., & Meijer, H.: Snow isotope diffusion rates measured in a laboratory experiment.
Journal of Glaciology, 57(201), 30-38. doi:10.3189/002214311795306727, 2011.

Van Geldern, R.; Barth, J.A.C.: Optimization of instrument setup and post-run corrections for oxygen and hydrogen stable isotope measurements of water by isotope ratio infrared spectroscopy (IRIS). Limnology and Oceanography-Methods, 10(12), 1024-1036, https://doi.org/10.4319/lom.2012.10.1024, 2012.

685